Next Energy 5 (2024) 100170

Contents lists available at ScienceDirect

Next Energy

journal homepage: www.sciencedirect.com/journal/next-energy

Research article

Experimental analysis of a sorption thermal energy storage for air heating and dehumidification in electric vehicles

Stefano De Antonellis[a], Luca Davide Marocco[a], Giorgio Tomaino[a], Francesco Romano[a], Luigi Calabrese[b,c], Angelo Freni[b,*]

[a] Department of Energy, Politecnico di Milano, Via Lambruschini 4, Milano 20156, Italy
[b] CNR ICCOM - Institute of Chemistry of Organometallic Compounds, Via G. Moruzzi, 1, Pisa 56124, Italy
[c] Department of Engineering, University of Messina, Contrada di Dio Sant'Agata, Messina 98166, Italy

ARTICLE INFO

Keywords:
Adsorption
Desiccant
Zeolite
Electric vehicle
Storage

ABSTRACT

Electric Vehicles (EVs) will play a crucial role in next years to reach the desired reduction of CO_2 emissions. One of the most critical aspects limiting the spread of this type of vehicle is the shorter range compared to conventional Internal Combustion Vehicles (ICVs). According to recent studies, in cold climate up to 50% of battery energy is used to control climate of passenger compartment.

This paper presents the design, development, and experimental analysis of a prototype open sorption Thermal Energy Storage (TES) system specifically engineered for air heating and dehumidification in EVs. The prototype includes 1 kg of zeolite 13X in spherical beads and a Positive Temperature Coefficient (PTC) heater for regeneration. Experimental results, conducted under representative winter conditions, indicate that the device can provide a dry and warm airflow for 45–90 minutes, depending on the mode of operation. Integrating this TES system into the vehicle's air handling unit significantly reduces the outdoor airflow rate without risk of window fogging. Simulations show that the device can reduce the thermal power required to heat the cabin by up to 50% during vehicle operation. During discharge, energy saving is approximately 1300 Wh when the outdoor temperature is 0 °C.

In conclusion, the proposed open sorption TES prototype demonstrates a viable approach to enhancing energy efficiency and passenger comfort in EVs.

1. Introduction

Currently, the transportation sector is responsible for 20% of total CO_2 emissions, with the majority stemming from road vehicles. Specifically, light-duty vehicles emitted 3 Gt CO_2 in 2020, with a target reduction to 2 Gt CO_2 by 2030 and nearly zero by 2050. Achieving this ambitious goal requires electric vehicle (EV) sales to reach 55 million by 2030, which is 18 times the number sold in 2020, leading to a gradual phase-out of internal combustion vehicles (ICVs) [5].

Based on the aforementioned considerations, EVs will play a crucial role in next years to reach the desired CO_2 emissions targets. One of the most critical aspects limiting the spread of this type of vehicle is the shorter range compared to conventional ICVs. According to recent studies, up to 50% of battery energy is used to control climate of the passengers compartment [22], to maintain comfortable thermo-hygrometric conditions, ensure indoor air quality and prevent windows fogging. It has been shown that even in mild climate conditions, such as at 8 °C, the energy consumption required to heat a sedan car passenger compartment can reduce its range by 40% [11]. Users of electric vehicles perceive this issue as particularly limiting, as they are used to drive cars with internal combustion engines in which the power required to heat the passenger compartment is provided by the engine itself, with no impact on range. Therefore, improving the heating, ventilating, and air conditioning (HVAC) system of EVs is particularly important to increase their range and promote their adoption.

Ongoing research deals with the improvement of vehicle HVAC system and vehicle envelope, as widely discussed in review papers [17,22,23]. In particular, studies about compartment heating are focused on: control and reduction of ventilation airflows, development of efficient heat pumps, improvement of vehicle envelop and glazing, development of thermal storage systems, design of hybrid vapor compression/adsorption system and integration of HVAC and battery thermal management.

* Corresponding author.
E-mail address: angelo.freni@pi.iccom.cnr.it (A. Freni).

https://doi.org/10.1016/j.nxener.2024.100170
Received 13 June 2024; Received in revised form 12 July 2024; Accepted 24 July 2024

Nomenclature

c_p	Specific heat at constant pressure [J kg^{-1} °C^{-1}]
h	Specific enthalpy [J kg^{-1}]
h_{ads}	Average heat of adsorption [J kg^{-1}]
k_{ENV}	Vehicle envelope overall heat transfer coefficient [W °C^{-1}]
M	Mass [kg]
$\dot{m}$	Mass flow [kg s^{-1}]
n	Quantity [-]
$\dot{Q}$	Power [W]
RH	Relative Humidity [-]
T	Temperature [°C]
t	Time [s]
$\dot{V}$	Volumetric dry air flow [m^3 h^{-1}]
X	Humidity Ratio [kg kg^{-1}]

Greek letters

λ	Enthalpy of evaporation of water [kJ kg^{-1}]
ρ	Density [kg m^{-3}]

Subscripts

a	Ambient (cabin) air condition
ads	Adsorption material
avg	Average value
ch	Charge process
da	Dry air
dis	Discharge process
e	External (outdoor) air condition
ENV	Vehicle envelope
in	Inlet
out	Outlet
p	Person
pp	Persons
PTC	PTC heater
rec	Recirculated
s	Supply air condition
S	Sensible
TES	Thermal Energy Storage
TH	Thermal
v	Water vapor
VENT	Ventilation
wa	Wet air
N	Reference air density (ρ = 1.2 kg m^{-3})

Acronyms

AHU	Air Handling Unit
EXP	Experimental
EV	Electric Vehicle
HVAC	Heating Ventilating and Air Conditioning
IAQ	Indoor Air Quality
ICV	Internal Combustion Vehicle
PTC	Positive Temperature Coefficient
PWM	Pulse With Modulation
TES	Thermal Energy Storage

Power required to heat interior compartment is related to both ventilation load and heat transfer through the vehicle envelope. Compartment ventilation with outdoor airflow is very important to control indoor air quality [2,9] and prevent windows fogging [3,14], thus ensuring safe conditions for the occupants [16]. In winter conditions, thermal load due to ventilation can be around 50% of total [19]. Therefore, an appropriate management of recirculated and outdoor airflows can effectively contribute to reduce the HVAC power consumption, keeping Indoor Air Quality (IAQ) and fogging as primary issues to be properly considered. Thermal loads through the envelope and windows can be reduced by applying insulation materials or using low conductive transparent materials [7]. Simulations results highlight that increased cabin insulation leads to a reduction of steady-state heating power by 3.8%–18.3%.

To increase heating power production efficiency, heat pumps technology is often adopted instead of electric resistances. Such technology is well known due to similarities with industrial and residential ones and with vehicle vapor compression refrigeration systems. Heat pumps can significantly reduce energy consumption compared to electric heaters even though performance in cold climates is strongly affected by outdoor temperature and, in particular, by frost formation on the evaporator, as discussed in several research studies [10,23,26].

A further approach investigated to reduce battery energy consumption deals with thermal energy storage (TES) systems: energy is stored when batteries are charged, and it is released into the passenger compartment when the vehicle is used. Several studies focus on TES based on phase change materials [1,23]: although these storage systems can contribute to reduce battery energy consumption, they are bulky and not intrinsically able to store heat for a long time, due to losses to the surrounding. TESs based on sorption phenomenon are of particular interest, as they allow to store energy for an indefinite period and to produce heating (or even cooling) on demand [17,18,23]. In particular, open desiccant systems are compact and light weight devices that can provide a warm/hot and dry airflow [4,25], heating the compartment and preventing windows fogging. Although the effectiveness of the device has already been demonstrated, there are still a number of technological limits (adsorbent selection, system configuration, management/regeneration logic, space optimization, etc.) that need to be addressed in order to promote the use of the system in the transport sector [12,15].

Finally, researchers are studying hybrid devices combining vapor compression and adsorption systems [17]. A closed adsorption system can substitute the compressor and provide refrigerant storage, reducing overall battery energy consumption [8]. Instead, an open adsorption technology is adopted to dehumidify the air stream supplied to the compartment and increase heat pump efficiency [13,24]. Although these approaches provide preliminary promising results, a significant effort to reduce complexity, weight and dimensions should still be done.

According to literature review, open sorption TESs can provide a significant contribution to improve HVAC systems of EVs in winter operation. In particular, these devices guarantee TES for an indefinite period and provide dehumidification and heating of an airflow. As a result, the outdoor airflow rate can be significantly reduced, leading to a substantial decrease in the heating power required to control the passenger compartment's air conditions. Open sorption TESs are widely studied in scientific literature for stationary systems and their effectiveness has been extensively demonstrated [4,20]. Anyway, this technology has not been investigated for vehicle applications and it presents several limitations such as: weight and dimensions, material cost, integration with conventional vehicle HVAC system, charge and discharge procedure. To contribute to the adoption of open sorption TES systems for vehicle applications, these issues must be thoroughly investigated and addressed. In this work, a prototype TES system was designed and manufactured. Extensive experimental tests were conducted under representative winter operating conditions, and the results were analyzed. Finally, preliminary simulations were performed to assess the benefits of integrating the device with the vehicle HVAC system.

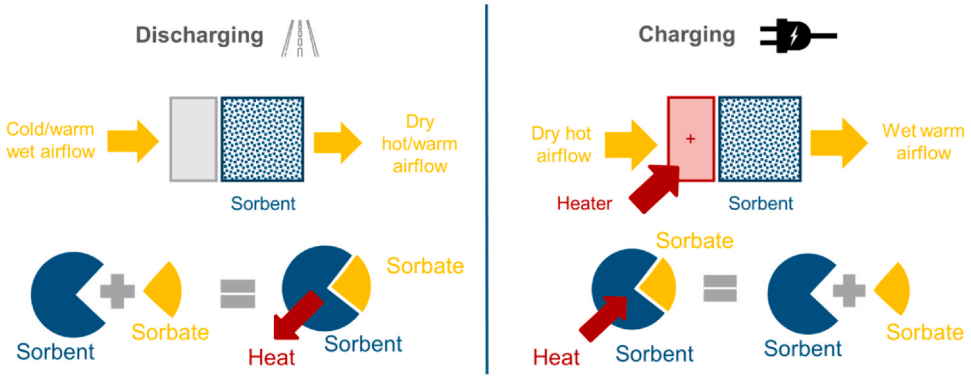

Fig. 1. Operating principle of open sorption TES. TES = thermal energy storage.

2. Thermal energy storage description and integration at vehicle level

The principle of charging and discharging process of open sorption TES systems is based on the reversible reaction between a sorbent (zeolite, silica gel, alumina, etc.) and a sorbate (water vapor), as shown in Fig. 1. The basic system consists of an adsorbent bed that is appropriately crossed by an airflow. During discharging, the cold-wet air stream flows through the bed: water vapor is adsorbed, and the airflow increases its temperature, due to the release of the heat of adsorption. During charging (regeneration) the sorbent is regenerated, and water vapor removed: a hot air stream goes through the sorbent bed to increase its temperature and, consequently, removes the adsorbed water. As a result, a warm and humid airflow leaves the bed. Between the charging and discharging processes, the sorbent is kept separated from the sorbate using flaps or dampers. As a result, the heating and dehumidification capacity remains available indefinitely.

The open sorption TES can be effectively used in EVs: charging of the sorbent is carried out at the same time as batteries are recharged. Electricity is used to heat an airflow and to regenerate the desiccant bed. The heating/dehumidification capacity is then exploited during normal vehicle use: an airflow passes through the adsorbent bed, where it is heated and dehumidified. Part of the heating load of the passenger compartment can be satisfied by the open TES, while the remaining load should be provided by the batteries through an electric resistance heater or a heat pump (reference technologies).

A possible integration of TES in the vehicle HVAC system is reported in Fig. 2. In Fig. 2A the reference HVAC unit is shown. Upstream of the fan, outdoor and recirculated airflows are properly mixed. Then, the resulting airflow is heated by the condenser (if available) and the post heating section, and supplied to the interior compartment through vents. In the other two drawings, a possible integration of the TES is described. During discharging (Fig. 2B), part of the airflow goes through the sorbent bed and is heated and dehumidified. Then, it is mixed again with the main airstream bypassing the TES. Due to the TES dehumidification capacity, the outdoor airflow can be significantly reduced compared to the reference condition (Fig. 2A), allowing it to be primarily regulated for indoor air quality control. During the device charging phase (Fig. 2C), outdoor airflow is utilized to regenerate the adsorbent. The Positive Temperature Coefficient (PTC) heater is activated to increase the air temperature, and the moist airflow exiting the sorbent bed is exhausted outside the vehicle.

3. Prototype and experimental setup description

3.1. Thermal energy storage prototype

The TES prototype, shown in Fig. 3, consists of the following components:

- A casing made of glass fiber-reinforced PPS, manufactured using filament fused deposition 3D printing technology.
- A PTC air heater (230 V AC), consisting of six insulated elements connected by aluminum fins.
- A sorption bed, consisting of 1 kg of zeolite 13 X beads.

The TES is designed to provide a discharge of 30–60 minutes, depending on operating conditions, as discussed in next Section 4. Air enters the device through the top opening and exits through the bottom

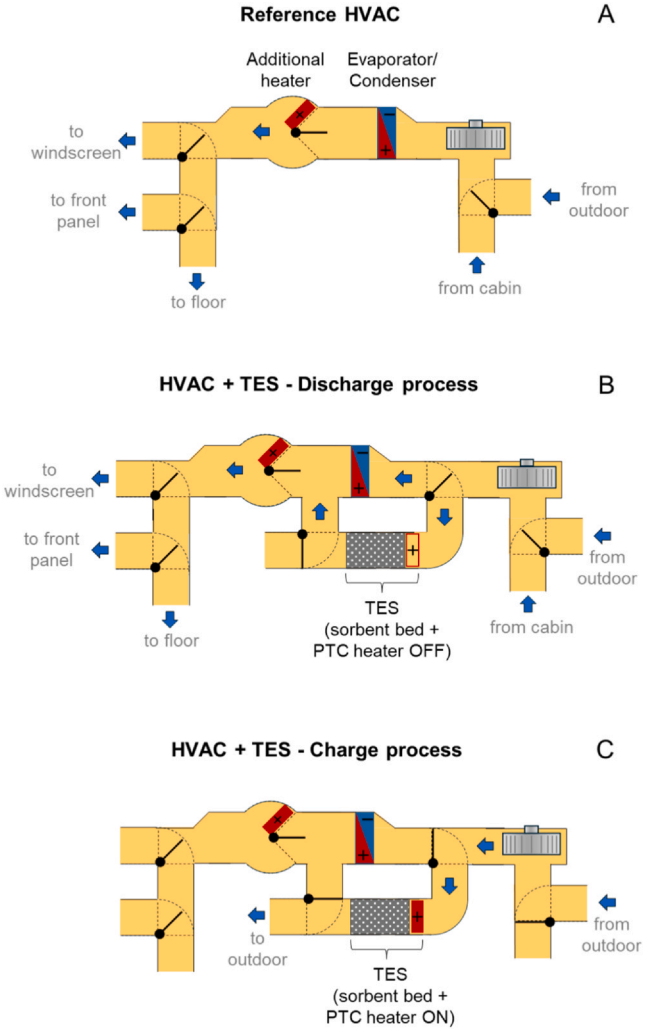

Fig. 2. Integration of open sorption TES in the vehicle HVAC system. HVAC = heating ventilating and air conditioning.

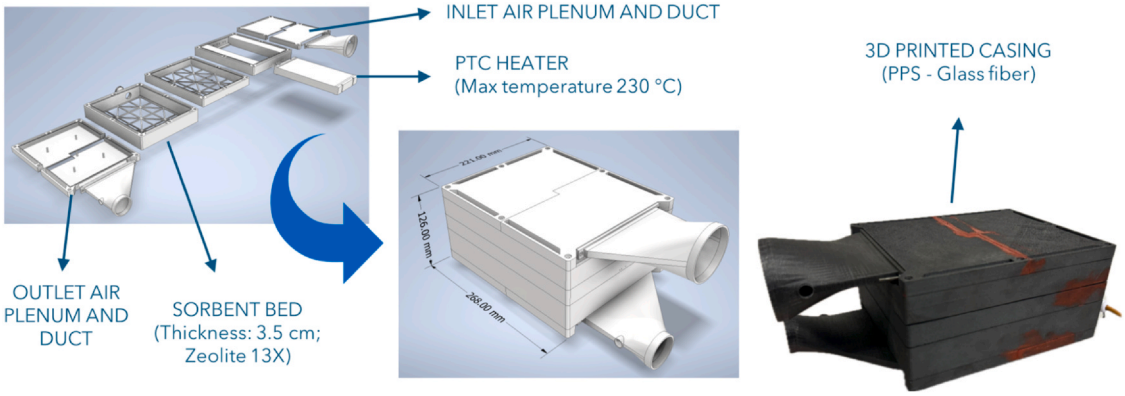

Fig. 3. Scheme and picture of open sorption TES.

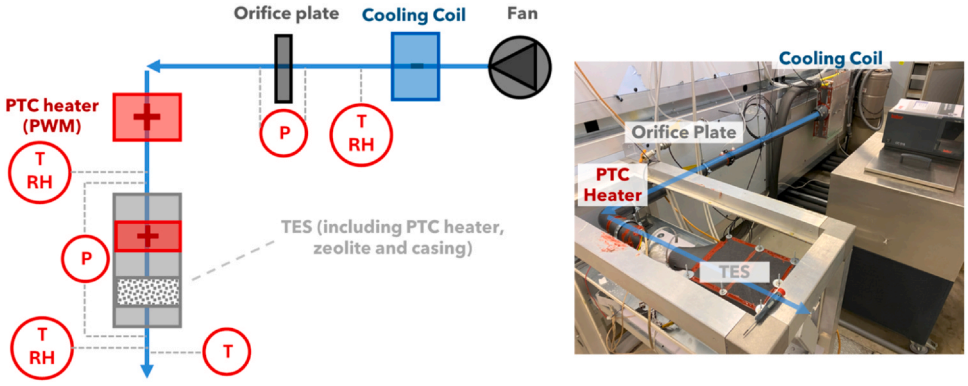

Fig. 4. Functional scheme and picture of the test rig.

one. In the lateral walls of the casing a small cavity (1 cm) is created to limit heat losses. The total casing volume, excluding the inlet and outlet ducts, is 7.4 Liters. The top and bottom plenums are insulated during tests with a 2 cm thick rockwool panel. The self-regulating PTC heater has a maximum surface temperature of 230 °C and a nominal power of 2570 W (with airflow rate equal to 300 $m^3\ h^{-1}$ and inlet air temperature equal to 20 °C). The zeolite bed has a thickness of 3.5 cm, with an average spherical beads diameter of 2 mm. The water vapor adsorption capacity is 26% at $T = 25$ °C and $RH = 75\%$ and bulk density is equal to 620 $kg\ m^{-3}$.

It should be noted that the dimensions of this prototype, which currently includes only the heater and the zeolite bed, are not optimized. In fact, there is unused space around the PTC heater and between it and the adsorbent bed. A prototype with an extended capacity (3–4 kg of zeolite) and an optimized geometry, including a dedicated fan and flaps, could have a volume around 10–12 Liters.

3.2. Test rig

The sorption thermal energy storage device was tested through a dedicated test rig, which provides an airflow at controlled temperature, relative humidity and flow rate. The setup consists of the following components:

- A variable speed fan.
- A cooling coil, connected to a chiller, to cool and dehumidify the airflow.
- An orifice plate, manufactured according to EN ISO 5167-2 international standard [6] and connected to piezo-resistive pressure sensors (± 0.5% of reading ± 1 Pa) to evaluate volumetric airflow (average uncertainty ± 3% of reading).
- An electric heating section, controlled through pulse with modulation (PWM) methodology, to set airflow temperature entering the TES.

As shown in Fig. 4, air conditions are measured through a PT100 temperature probe (± 0.3 °C at 20 °C, max operating temperature of 160 °C) and coupled PT100 thermo-resistances (± 0.2 °C at 20 °C, max operating temperature of 120 °C) along with relative humidity capacitive sensors (± 1% at 20 °C), installed in the test rig ducts. The electric power consumption of the PTC heater in the TES prototype is measured using a programmable transducer (± 0.5% of reading). Additionally, a piezoresistive pressure sensor (± 0.5% of reading ± 1 Pa) is installed between the TES entrance and exit to evaluate device pressure drops in a dedicated test rig.

4. Experimental analysis of TES

4.1. Adopted methodology

The TES prototype was tested under typical winter conditions to assess its performance in a real operating environment. Several tests were conducted at low temperature and low humidity ratio conditions, which are not commonly investigated in the literature. Unless otherwise specified, the TES discharge process was carried out at least 12 hours (one night) after the completion of the charge process (regeneration via the PTC heater until steady state conditions were reached), allowing the device temperature to cool down to laboratory conditions (approximately 22 °C). During this cooling period, as well as every time between charging and discharging, both the inlet and outlet TES ducts were sealed with airtight caps.

In Section 4.2, relevant trends during the discharge and charge process are reported and discussed, to clarify the device performance. In addition, the power consumption of TES PTC heater is independently evaluated. In Sections 4.3 and 4.4, the effect of different inlet airflow conditions during discharge and charge are evaluated. During each test, temperature, humidity ratio and airflow rate are maintained constant, according to the values reported in Table 1 (with the following

Table 1
Conditions of experimental tests

Test	Discharging				Charging				Duct caps
	$T_{in,dis}$ [°C]	$X_{in,dis}$ [g kg^{-1}]	$\dot{V}_{dis,N}$ [m^3 h^{-1}]	t_{dis} [s]	$T_{in,ch}$ [°C]	$X_{in,ch}$ [g kg^{-1}]	$\dot{V}_{ch,N}$ [m^3 h^{-1}]	t_{ch} [s]	
REF	21	4	20	max	6.5	4	20	max	yes
A	21	4	30	max	6.5	4	20	max	yes
B	6.5	4	20	max	6.5	4	20	max	yes
C	−2.5	2	20	max	6.5	4	20	max	yes
D	21	4	20	max	6.5	4	30	max	yes
E	21	4	20	max	21	4	20	max	yes
F	21	4	20	max	−1	2	20	max	yes
G	21	4	20	max	6.5	4	20	1500[a]	yes
H	21	4	20	max	6.5	4	20	max	yes
I	21	4	20	2700[b]	6.5	4	20	max	no
L	21	4	20	max	-	-	-	no[c]	no

[a] Charge process is suspended after 1500 s.
[b] Discharge process is suspended after 2700 s.
[c] No sorbent regeneration (charge). Discharge is performed four days after partial discharge of test I.

tolerance: ± 0.5 °C, ± 0.2 g kg^{-1}, ± 1 m^3 h^{-1}). Finally, in Section 4.5 the TES storage capacity over time is discussed.

4.2. Discharge and charge process

In Figs. 5A and 5B, the temperature and humidity ratio profiles during the discharge period are shown. During the first 30 minutes, the adsorption capacity of the bed reaches its maximum, while the humidity ratio $X_{out,dis}$ at the TES outlet is less than 0.1 g kg^{-1}. At the same time, there is an increase in outlet temperature $T_{out,dis}$ due to the release of adsorption heat. Subsequently, as the adsorption capacity of the zeolite decreases, a corresponding decrease in $T_{out,dis}$ and an increase in $X_{out,dis}$ are observed. In addition to instrumental uncertainty of directly measured quantities provided in Section 3.2, during the discharge the maximum value of combined uncertainty of X_{out} is ± 0.4 g kg^{-1}. In Fig. 5C, the mass flow rate of adsorbed water $\dot{m}_{v,dis}$ and the total amount of adsorbed water over time $M_{v,dis}$ are reported, defined as follows:

$$\dot{m}_{v,dis} = \dot{m}_{da,dis}(X_{in,dis} - X_{out,dis}) \quad (1)$$

$$M_{v,dis} = \int_0^t \dot{m}_{v,dis}\,dt \quad (2)$$

The flow rate of the adsorbed water is initially equal to 97 g h^{-1} (uncertainty of ± 4 g h^{-1}) and it remains almost constant until the adsorption capacity of the material begins to decrease, reaching zero as the process concludes. Overall, the amount of water $M_{v,dis}$ removed from the wet airflow is 178 g. It can be reasonably assumed that in real applications, the maximum water content will settle around 150 g. Above this value, due to the increase of $X_{out,dis}$, it would be necessary to significantly increase the air flow rate in order to maintain a constant dehumidification capacity.

In Figs. 6A and 6B, the temperature and humidity ratio profiles during discharge are shown. Initially, the air temperature increases due to the power released by the PTC heater, which is activated during this process. At the same time, the outlet humidity ratio increases as the zeolite beads begin to desorb water. Then, a flat zone is observed where $T_{out,ch}$ and $X_{out,ch}$ remain approximately constant, during which condensation of vapor occurs in the outlet plenum ($RH_{out,ch}$ = 100%). This zone persists until the TES structure and the zeolite are sufficiently heated. Finally, for t > 700 s, outlet air temperature increases and humidity ratio decreases, indicating the progressive reduction of water content in the zeolite beads. The trend of the humidity ratio stops at t = 2150 s because the sensor reached its maximum operating temperature. In addition, it should be noticed that at high temperature the uncertainty of the calculated humidity ratio is very high. For instance, in the charge test when $T_{out,ch}$ approaches 100 °C, the uncertainty of $X_{out,ch}$ is around ± 7 g kg^{-1}. Finally, in Fig. 6C, the power consumption of the PTC heater $\dot{Q}_{PTC}$ during TES regeneration is shown. The power consumption remains constant except during the initial phase, during which the heater warms up. The total energy consumed E_{PTC} is calculated as follows:

$$E_{PTC} = \int_0^t \dot{Q}_{TES}\,dt \quad (3)$$

At the end of the charging process, the measured energy consumption is 850 Wh. However, such value can be significantly reduced by: i) reducing the air flow rate, as discussed more in detail in Section 4.3; ii) introducing a heat exchanger between the inlet and outlet of the TES, so that the air preheats; iii) reducing the regeneration time. In particular, with regard to the last approach, it can be observed that after 2700 s the regeneration is almost completed, as $T_{out,ch}$ has practically already reached its maximum value.

Fig. 7 shows the power consumption of the PTC heater of the TES for different airflow rates and temperatures. The electrical resistance of the heater varies with its temperature, which is influenced by the airflow rate and its temperature. Specifically, as the airflow rate increases, the surface temperature of the heater decreases, leading to an increase in electrical power consumption. However, it is important to note that the increase in power consumption is proportionally smaller than the increase in airflow rate. Consequently, as the airflow rate rises, the outlet air temperature decreases.

The maximum surface temperature is 230 °C, ensuring the device intrinsically safe in the event of a failure. The test results align with the trends provided by the manufacturer for higher airflow rates than those used in this study.

Finally, the pressure drop of the TES prototype was measured through the differential pressure sensor installed between the air inlet and outlet section (Fig. 4). When the flow rate $\dot{V}_N$ was 20 m^3 h^{-1} and 40 m^3 h^{-1}, the measured pressure drop were 118 Pa and 400 Pa respectively.

4.3. Effect of discharge conditions

Fig. 8 compares different discharge processes of the TES prototype, in which the charge process was performed under the same operating conditions, as shown in Table 1. Compared to the reference case (Test REF), if the airflow rate is increased (Test A), a reduction in discharge duration is observed due to the faster saturation of the sorbent material.

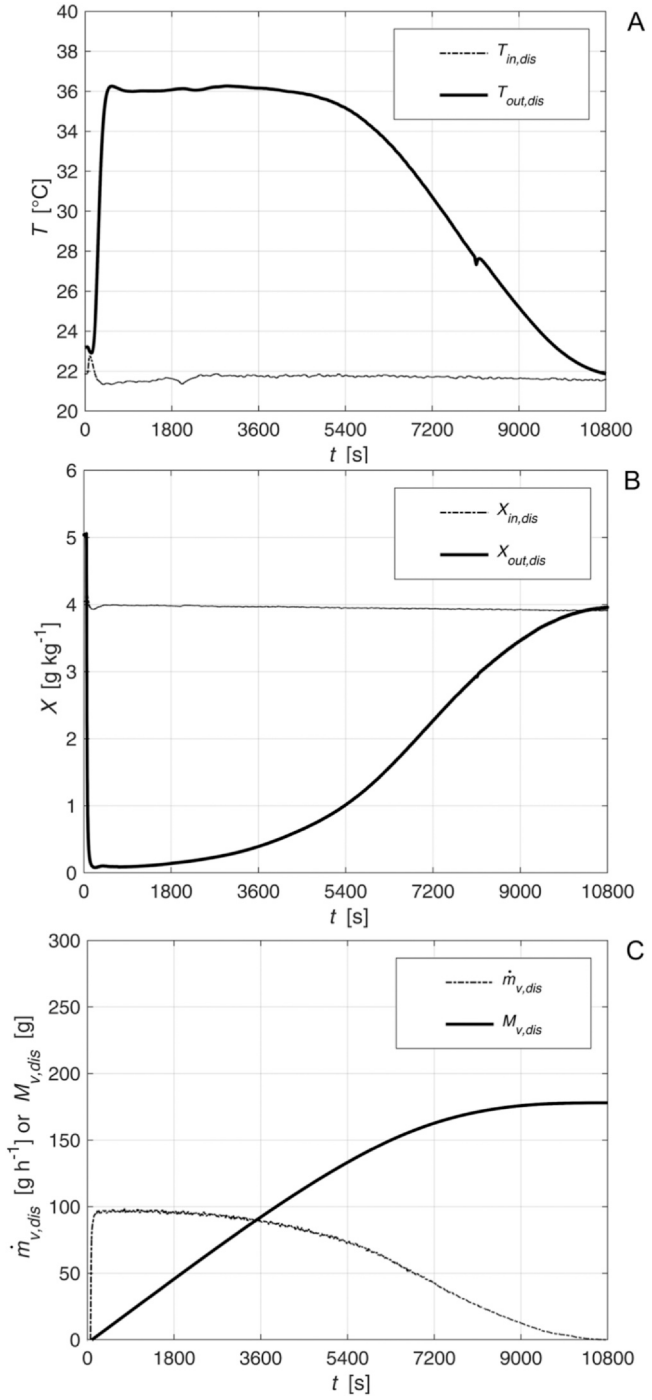

Fig. 5. Discharge process of TES (Test REF of Table 1).

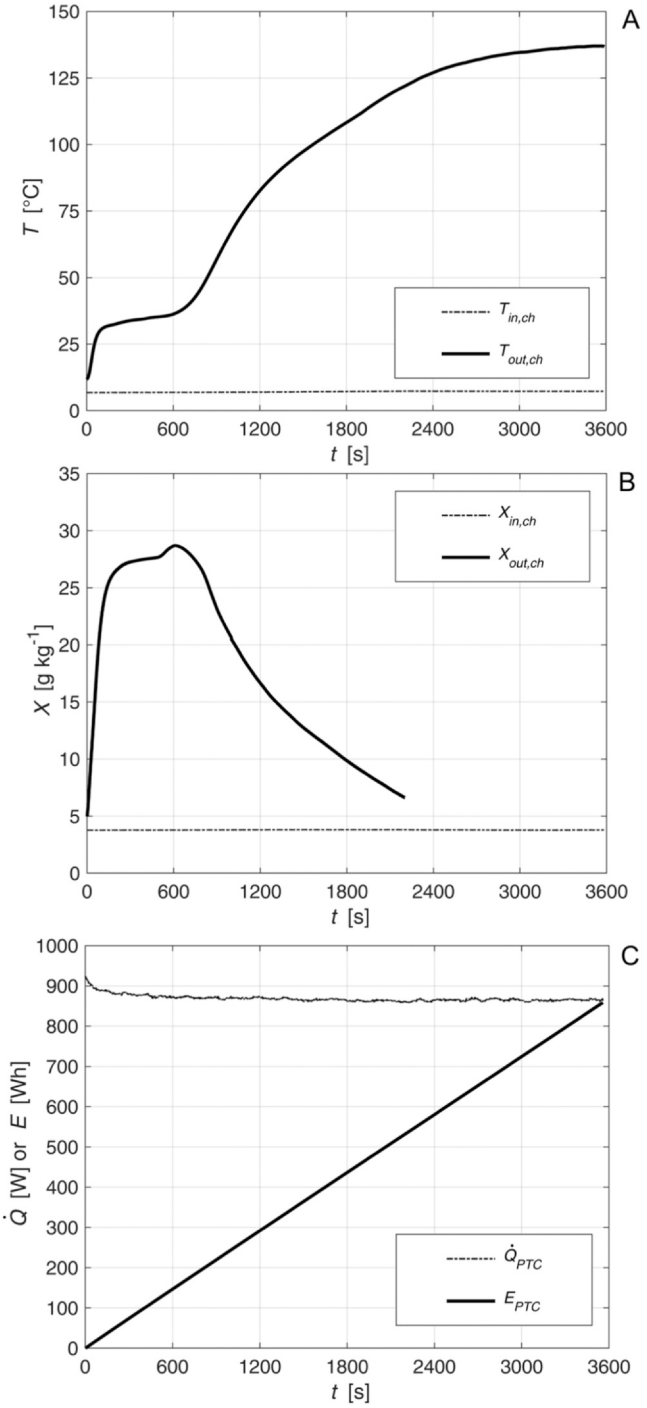

Fig. 6. Charge process of TES (Test REF of Table 1).

The maximum adsorbed water content, on the other hand, does not change, as it depends only on inlet air conditions T_{in} and X_{in} during both charge and discharge processes. Conversely, a lower $T_{in,dis}$ (Test B) leads to a corresponding lower $T_{out,dis}$. This results in higher relative humidity along the TES compared to the reference case, enhancing the sorbent adsorption capacity. Consequently, this effect produces a slightly lower outlet humidity ratio profile over time and a higher water content $M_{v,dis}$ at the process conclusion compared to the reference case. Finally, when both $T_{in,dis}$ and $X_{in,dis}$ decrease simultaneously (Test C), the following effects are observed: i) a reduction in $T_{out,dis}$, due to both the lower $T_{in,dis}$ and the lower release of the heat of adsorption; ii) a decrease in $X_{out,dis}$, due to the reduction in $X_{in,dis}$; iii) an increase in the duration of the discharge process, due to the lower content of adsorbed water over time.

The aforementioned considerations highlight that, under the same regeneration conditions, the performance of the TES system during discharge is highly dependent on the inlet air conditions. In particular, low values of temperature and humidity ratio, typical of winter conditions, allow to increase the adsorbed water content and the discharge duration of the device.

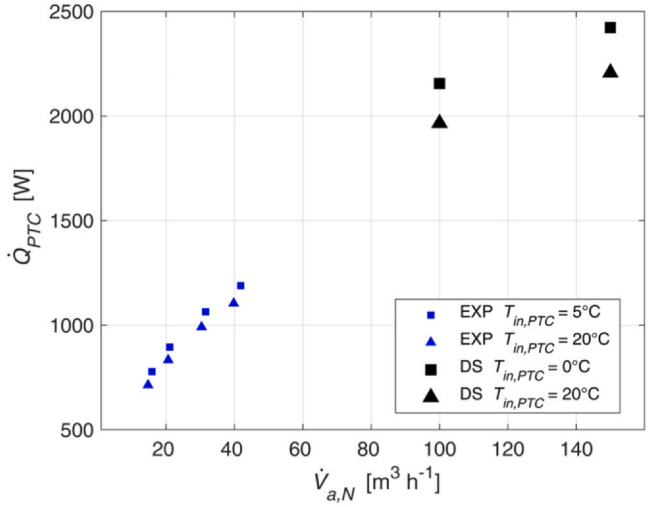

Fig. 7. Power consumption of TES PTC heater (EXP: experimental test; DS: Manufacturer datasheet). PTC = Positive Temperature Coefficient.

4.4. Effect of charge conditions

In Fig. 9, the effect of charging air conditions on the discharge process, performed in the same way, are shown. In Test D, with higher $\dot{m}_{da,ch}$, the air temperature at the PTC heater outlet (as discussed in Section 4.2) decreases, resulting in a less effective regeneration process. Consequently, during discharge, $M_{v,dis}$ and duration decreases. In Test E, if $T_{in,ch}$ increases, there is a slight increase in the regeneration temperature: in Fig. 9C it is shown that the adsorbed water content at the end of the process is only slightly higher than in Test REF. On the other hand, the profiles of $T_{out,dis}$ and $X_{out,dis}$ are slightly different from the reference case due to the slightly different inlet air temperature and humidity ratio (within the limits given in Section 4.1). In Test F, the regeneration of the prototype is carried out with a lower inlet air temperature and humidity ratio. Overall, as discussed for Test E, the effects on the discharge process are negligible, with trends of $T_{out,dis}$, $X_{out,dis}$ and $M_{v,dis}$ similar to those of Tests REF and Test E. Finally, in Test G the regeneration is stopped after t_{ch} = 1500 s instead of waiting for equilibrium (t_{ch} > 3600 s). Consequently, the adsorbent material's regeneration is incomplete, leading to reduced discharge performance. Notably, the energy consumption for sorbent regeneration is approximately 350 Wh (compared to 850 Wh in Test REF), while the amount of water adsorbed is 150 g (compared to 180 g in Test REF). Therefore, a well-considered regeneration strategy, based on appropriate airflow rates and cycle times, can significantly reduce energy consumption during the charging phase.

4.5. Storage capacity over time

Finally, some tests were carried out to assess the TES capability to store energy over time. As already described in Section 2, the operating principle of the TES system is based on the phenomenon of physical adsorption. The device remains charged over time as long as the vapor in the air does not come into contact with the zeolite. Therefore, the air-tightness of the device flaps and the diffusion of water vapor inside it significantly impact this capability. Fig. 10 shows discharge tests carried out as a result of regeneration processes with the same $T_{in,ch}$, $X_{in,ch}$ and $\dot{V}_{ch,N}$:

- REF: Reference case in this study, where discharge occurred 12 hours after regeneration. Air-tight caps are installed between charge and discharge process.
- Test H: Discharge took place four days after regeneration. Air-tight caps are installed between charge and discharge process.

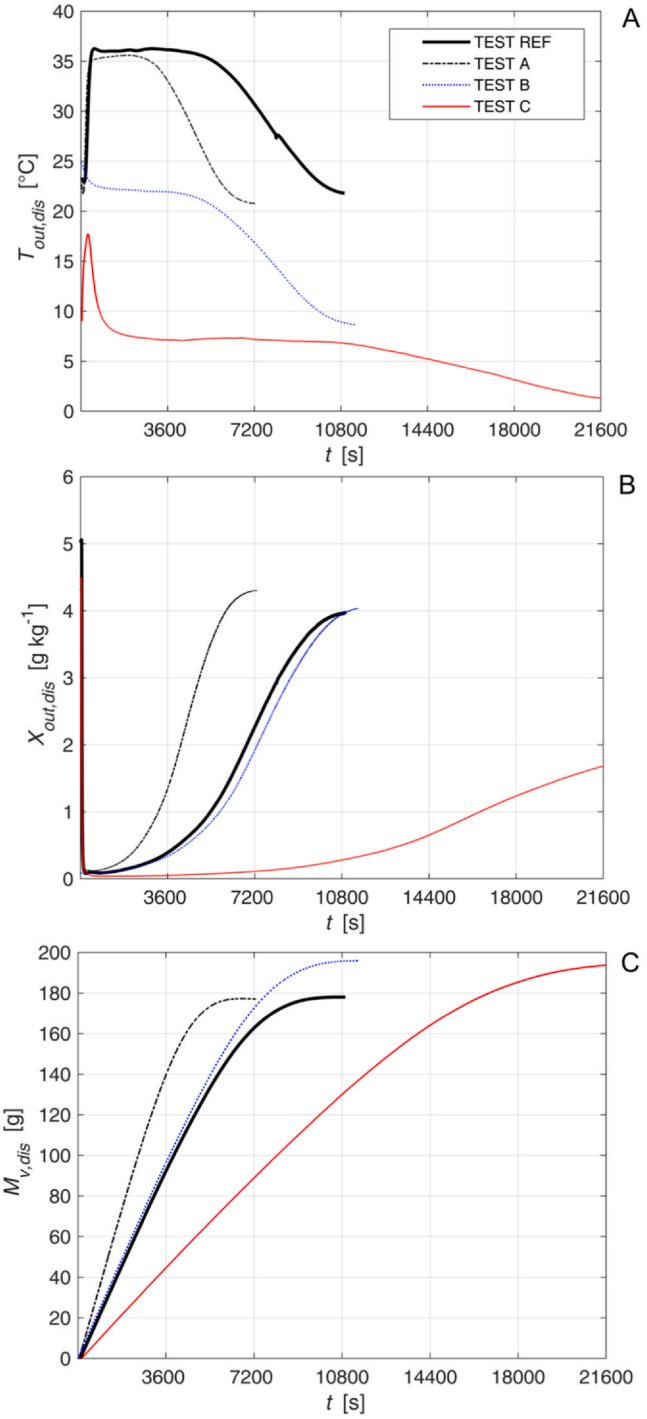

Fig. 8. Effect of discharge operating conditions on TES performance.

- Test I: Discharge occurred eight days after regeneration. No caps installed. The discharge process was halted after 45 minutes.
- Test L: Following Test I, discharge occurred four days after its interruption, without further regeneration. No caps installed.

As shown in Fig. 10, when the inlet and outlet ducts are airtight (demonstrated by the overlapping curves of Test REF and H), the TES prototype maintains its charging capacity over time. Conversely, if the system is not isolated (a configuration that may reflect real-world scenarios with limited dampers/flaps), there is a slight decrease in the adsorption capacity of the bed. In addition, observing the trend of $M_{v,dis}$

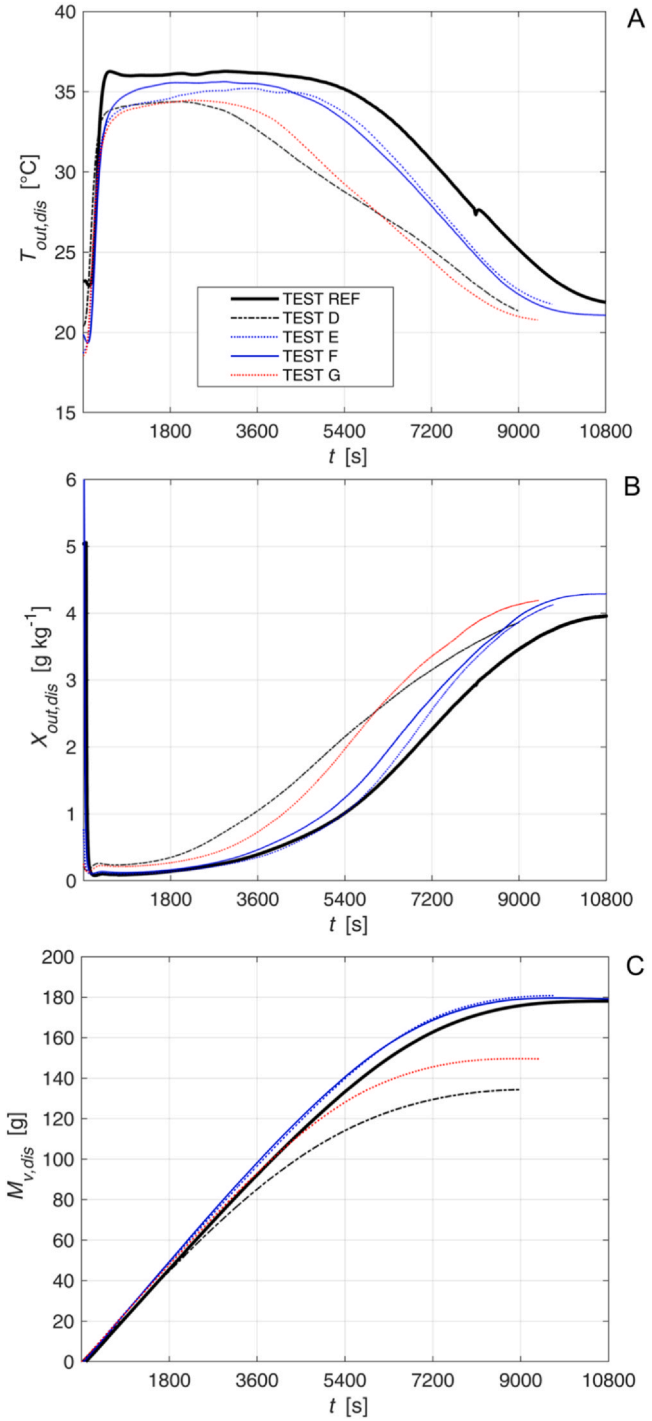

Fig. 9. Effect of charge operating conditions on TES performance.

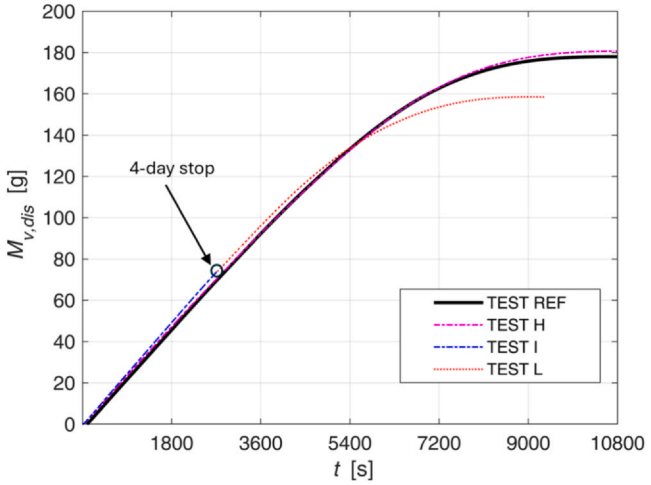

Fig. 10. Effect of storage conditions on TES performance.

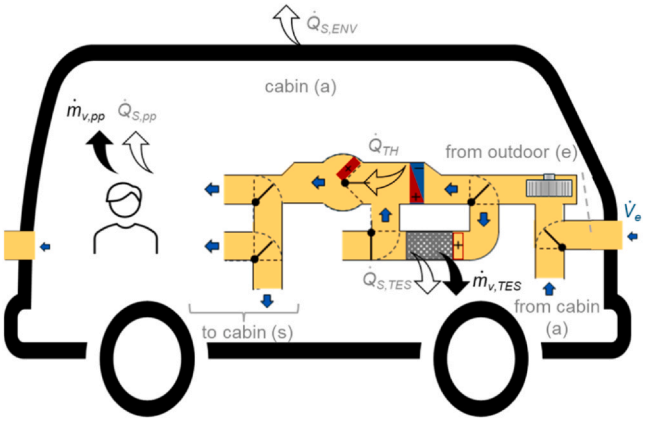

Fig. 11. Scheme representing sensible power, air and water vapor flows in the passenger compartment.

during Test I and Test L, it is evident that after a 4-day interruption, the device resumes its normal adsorption behavior.

5. Analysis at vehicle level

5.1. Ventilation load

In Fig. 11, a representation of exchanged powers and flow rates of dry air and water vapor in vehicle cabin are shown. Such terms are considered in the energy and mass conservation balances discussed in this TES analysis at vehicle level. As already mentioned in Section 1, introducing outdoor airflow is essential to dilute contaminants generated by occupants, to maintain a slight overpressure in the passenger compartment, and to mitigate the rise in CO_2 concentration and ambient humidity ratio.

In steady-state conditions, based on water mass balance inside the passenger compartment, the increase in humidity ratio between the outside and inside (ambient) air is:

$$X_a - X_e = \frac{\dot{m}_{v,pp} + \dot{m}_{v,TES}}{\dot{m}_{da,e}} \tag{4}$$

In the above equation, $\dot{m}_{v,pp}$ is the water vapor flow rate generated by people, $\dot{m}_{v,TES}$ is the flow rate removed from the TES system (which assumes a negative value if the device is present) and $\dot{m}_{da,e}$ is the mass flow rate of outdoor dry air (equal to $\dot{V}_{e,N}\ \rho_N/3600$). During winter period, it is necessary to limit the term X_a–X_e to prevent condensation on internal surfaces. To achieve this goal, an adequate outdoor airflow rate should be used. If the TES system is present, such airflow rate can be reduced keeping the same X_a–X_e.

The ventilation sensible power, i.e. the thermal power to raise the temperature from outdoor to cabin condition, is directly proportional to $\dot{m}_{da,e}$ and can be expressed as:

$$\dot{Q}_{S,VENT} = \dot{m}_{da,e} c_{p,wa,avg} (T_a - T_e) \tag{5}$$

Therefore, an adequate flow rate of outdoor air is necessary to limit humidity ratio in the passenger compartment. However, this also significantly impacts thermal power consumption. Substituting Eq. (4) in Eq. (5), $\dot{Q}_{S,VENT}$ is expressed as:

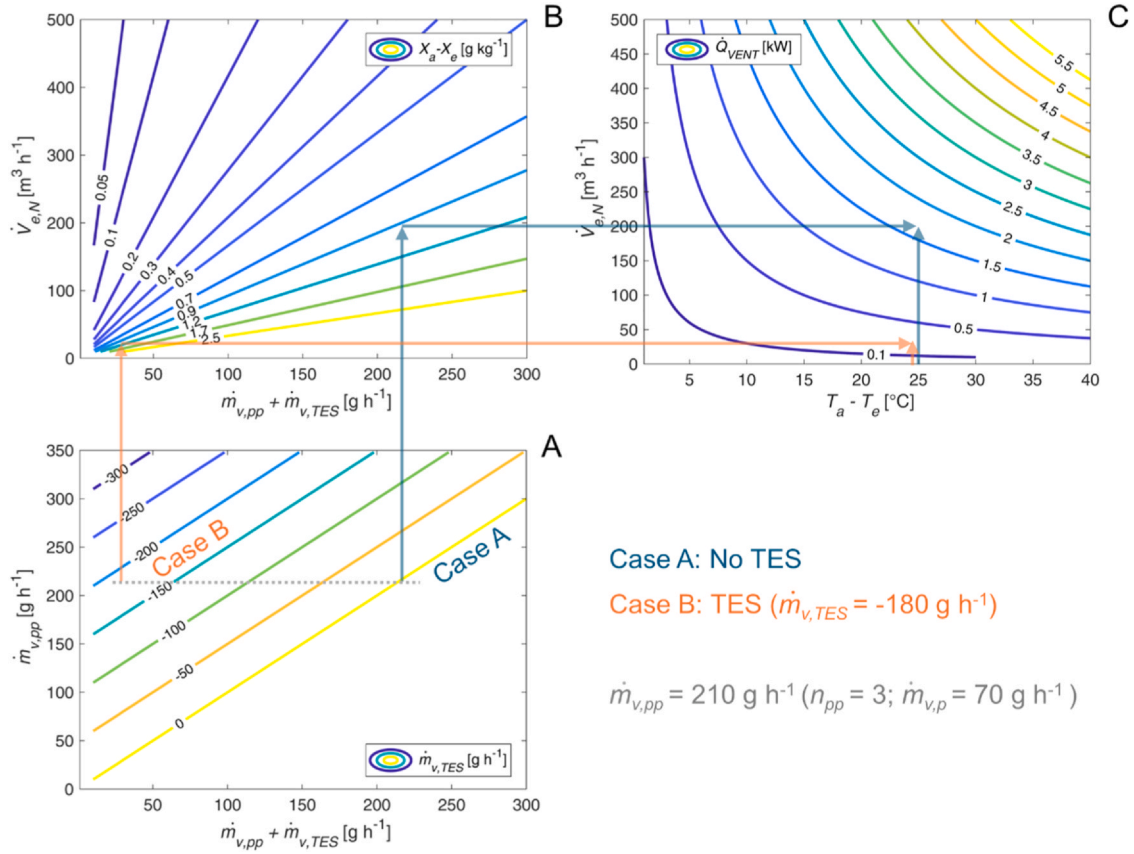

Fig. 12. Effect of TES dehumidification capacity on outdoor airflow rate and ventilation power.

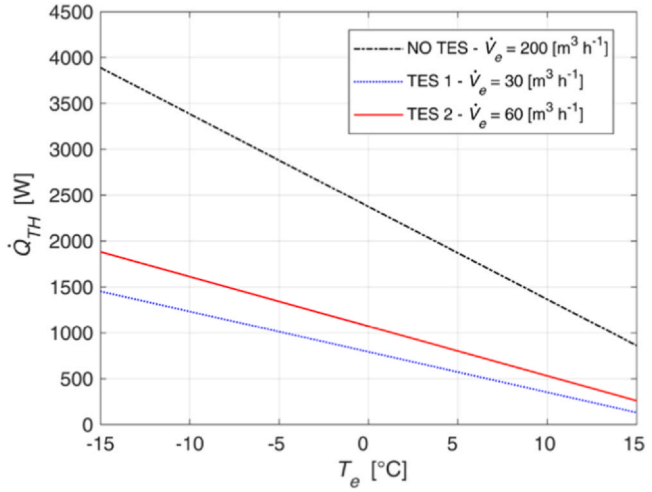

Fig. 13. Effect of outdoor air temperature on thermal power for different AHU configurations. AHU = Air Handling Unit.

$$\dot{Q}_{S,VENT} = \frac{\dot{m}_{v,pp} + \dot{m}_{v,TES}}{X_a - X_e} c_{p,wa,avg} (T_a - T_e) \tag{6}$$

It turns out that, to maintain X_a–X_e at a desired value, as the dehumidification capacity of the TES increases, the ventilation power decreases (with $\dot{m}_{v,TES}$ being a negative value). Fig. 12 shows two cases that highlight it: i) Case A, reference configuration without TES; ii) Case B, configuration with TES. In both cases, it is assumed that there are three persons in the vehicle, generating a total latent load $\dot{m}_{v,pp}$ = 210 g h^{-1} (Fig. 12A). In Case A, due to an external air flow rate $\dot{V}_{e,N}$ = 200 m^3 h^{-1}, it is possible to maintain a humidity ratio difference of 0.87 g kg^{-1}. In Case B, due to the presence of a TES device capable of removing 180 g h^{-1} of water vapor, an outside airflow rate around 30 m^3 h^{-1} is sufficient (Fig. 12B). This significant reduction in $\dot{V}_{e,N}$ leads to a decrease in ventilation power, dropping from 1.66 kW in Case A to 0.25 kW in Case B (Fig. 12C) when T_a–T_e is equal to 25 °C. Obviously, a minimum outdoor airflow must always be ensured to maintain IAQ and the pressurization of the passenger compartment. It should be noted that the prototype made in the framework of this research, based on 1 kg of zeolite, could provide the dehumidification capacity hypothesized for Case B (180 g h^{-1}) for approximately 45–50 minutes. This assumes that the system is considered exhausted and requires regeneration once a water content of 150 g is reached (as discussed in Section 4.2). Other operating conditions can be quickly evaluated by analogy using the diagram in Fig. 12.

5.2. Thermal power for cabin heating

Referring again to Fig. 11, under steady state conditions, the thermal power to be supplied by the Air Handling Unit (AHU) of the vehicle equals the sum of the power for ventilation and losses through the vehicle envelope, minus the contribution of the TES system (if present) and the internal thermal loads [21]:

$$\dot{Q}_{TH} = \dot{Q}_{S,VENT} + \dot{Q}_{S,ENV} - \dot{Q}_{S,pp} - \dot{Q}_{S,TES} \tag{7}$$

Where:

$$\dot{Q}_{S,ENV} = k_{ENV} (T_a - T_e) \tag{8}$$

$$\dot{Q}_{S,pp} = \dot{Q}_{S,p} n_{pp} \tag{9}$$

$$\dot{Q}_{S,TES} = h_{ads} \dot{m}_{v,TES} \tag{10}$$

It should be noted that solar radiation is neglected in this analysis, as the focus is on winter conditions. Fig. 13 shows the $\dot{Q}_{TH}$ value for different outdoor temperatures. The following assumptions were made:

medium-sized vehicle (k_{ENV} = 34 W °C^{-1}), presence of three people (n°_{pp} = 3 pp, $\dot{Q}_{S,p}$ = 50 W pp^{-1}), cabin temperature T_a = 25 °C and average heat of adsorption h_{ads} = 3200 kJ kg^{-1}. Three cases were considered: i) NO TES: $\dot{V}_{e,N}$ = 200 m^3 h^{-1} and absence of TES; ii) TES 1: $\dot{V}_{e,N}$ = 30 m^3 h^{-1} and presence of TES; iii) TES 2: $\dot{V}_{e,N}$ = 60 m^3 h^{-1} and presence of TES. The flow rate of water vapor removed by the TES is set to maintain the same humidity ratio as in the NO TES case. As can be seen from Fig. 13, $\dot{Q}_{TH}$ decreases by more than 50% in both cases. Clearly, the lower $\dot{V}_{e,N}$, the lower $\dot{Q}_{TH}$, but the value cannot be excessively low to maintain an adequate level of IAQ. Therefore, the TES system enables a significant reduction in energy consumption for winter air conditioning of the vehicle passenger compartment. Considering that in the TES 1 and TES 2 cases the water vapor removed by the TES is 180 g h^{-1} and 150 g h^{-1} respectively, it can be concluded that the prototype would last 50 and 60 minutes, respectively (assuming a maximum quantity of water before regeneration of 150 g and the presence of 1 kg of zeolite, as discussed in Section 4.2). At T_e = 0 °C, the TES saves about 1300 Wh, compared to 850 Wh spent for its regeneration (a value that, as discussed in Section 4.3, can be significantly reduced with appropriate approaches). To extend the discharge time of the TES, it is necessary to increase the amount of zeolite. For instance, using 3 kg of zeolite can extend the operation of the device to 2.5–3 hours, which is satisfactory for a typical vehicle. It should be noted that once the TES charge runs out, comfort conditions in the passenger compartment can still be maintained by operating the HVAC system in a conventional mode.

6. Conclusions

In this work, a prototype thermal energy storage system for electric vehicles, utilizing sorption materials, was developed. The device integrates a bed containing 1 kg of zeolite 13X and a PTC heater for its regeneration. The system heats and dehumidifies the air, allowing for a reduction in outdoor airflow. Consequently, there is a significant decrease in the power required to heat the vehicle cabin under winter conditions. Based on experimental tests and preliminary simulations, it was found that the thermal power required to heat passenger compartment in winter can be reduced by 50%. The developed prototype can save approximately 1300 Wh when the outdoor temperature is 0 °C, while energy required for regeneration is 850 Wh (a maximum value that can be significantly reduced). These results suggest that the TES can significantly contribute to increasing the range of electric vehicles in winter conditions and promote their adoption.

Declaration of Competing Interest

The authors declare that they have no known competing financial interests or personal relationships that could have appeared to influence the work reported in this paper.

Acknowledgment

We acknowledge partial financial support by PRIN 2022 – National Recovery and Resilience Plan (NRRP), Mission 4, Component 2, Investment 1.1, Call for tender No. 104 published on 2.2.2022 by the Italian Ministry of University and Research (MUR), funded by the European Union – NextGenerationEU – Project Title ACE-STES – CUP J53D23002370006. The authors also thank the European Union—NextGenerationEU (National Sustainable Mobility Center CN00000023, Italian Ministry of University and Research Decree n. 1033-17/06/2022, Spoke 11—Innovative Materials & Lightweighting).

References

[1] L.F. Cabeza, A. Solé, C. Barreneche, Review on sorption materials and technologies for heat pumps and thermal energy storage, Renew. Energy 110 (2017) 3–39, https://doi.org/10.1016/j.renene.2016.09.059.
[2] T.-B. Chang, J.-J. Sheu, J.-W. Huang, Y.-S. Lin, C.-C. Chang, Development of a CFD model for simulating vehicle cabin indoor air quality, Transp. Res. Part D: Transp. Environ. 62 (2018) 433–440, https://doi.org/10.1016/j.trd.2018.03.018.
[3] Davis, L.I., Dage, G.A., Hoeschele, J.D., 2001. Conditions for incipient windshield fogging and anti-fog strategy for automatic climate control. Presented at the SAE 2001 World Congress, pp. 2001-01–0583. https://doi.org/10.4271/2001-01-0583.
[4] S. De Antonellis, L.P.M. Colombo, P. Castellazzi, A. Rossetti, L. Marocco, System integration analysis of a zeolite 13x thermal energy storage, Energy Built Environ. 5 (2024) 568–579, https://doi.org/10.1016/j.enbenv.2023.04.006.
[5] IEA, 2021. Net zero by 2050 - a roadmap for the global energy sector.
[6] ISO, 2003. EN ISO 5167-2: 2022 measurement of fluid flow by means of pressure differential devices inserted in circular cross-section conduits running full.
[7] M.A. Jeffers, L. Chaney, J.P. Rugh, Climate control load reduction strategies for electric drive vehicles in cold weather, SAE Int. J. Passeng. Cars - Mech. Syst. 9 (2016) 75–82, https://doi.org/10.4271/2016-01-0262.
[8] L. Jiang, R.Z. Wang, J.B. Li, L.W. Wang, A.P. Roskilly, Performance analysis on a novel sorption air conditioner for electric vehicles, Energy Convers. Manag. 156 (2018) 515–524, https://doi.org/10.1016/j.enconman.2017.11.077.
[9] H.S. Jung, M.L. Grady, T. Victoroff, A.L. Miller, Simultaneously reducing CO_2 and particulate exposures via fractional recirculation of vehicle cabin air, Atmos. Environ. 160 (2017) 77–88, https://doi.org/10.1016/j.atmosenv.2017.04.014.
[10] S. Kwon, D. Lee, J.Y. Chung, H. Maeng, Y. Kim, Performance comparison of a direct heat pump using R1234yf and indirect heat pumps using R1234yf and R290 designed for cabin heating of electric vehicles, Energy 297 (2024) 131311, https://doi.org/10.1016/j.energy.2024.131311.
[11] D. Leighton, Combined fluid loop thermal management for electric drive vehicle range improvement, SAE Int. J. Passeng. Cars - Mech. Syst. 8 (2015) 711–720, https://doi.org/10.4271/2015-01-1709.
[12] B. Michel, P. Neveu, N. Mazet, Comparison of closed and open thermochemical processes, for long-term thermal energy storage applications, Energy 72 (2014) 702–716, https://doi.org/10.1016/j.energy.2014.05.097.
[13] S.-I. Na, Y. Chung, M.S. Kim, Performance analysis of an electric vehicle heat pump system with a desiccant dehumidifier, Energy Convers. Manag. 236 (2021) 114083, https://doi.org/10.1016/j.enconman.2021.114083.
[14] L. Pan, C. Liu, Z. Zhang, T. Wang, J. Shi, J. Chen, Energy-saving effect of utilizing recirculated air in electric vehicle air conditioning system, Int. J. Refrig. 102 (2019) 122–129, https://doi.org/10.1016/j.ijrefrig.2019.03.018.
[15] L. Scapino, H.A. Zondag, J. Van Bael, J. Diriken, C.C.M. Rindt, Sorption heat storage for long-term low-temperature applications: a review on the advancements at material and prototype scale, Appl. Energy 190 (2017) 920–948, https://doi.org/10.1016/j.apenergy.2016.12.148.
[16] Tsutsumi, H., Hoda, Y., Tanabe, S., Arishiro, A., 2007. Effect of car cabin environment on driver's comfort and fatigue. Presented at the SAE World Congress & Exhibition, pp. 2007-01–0444. https://doi.org/10.4271/2007-01-0444.
[17] S. Vashisht, D. Rakshit, Recent advances and sustainable solutions in automobile air conditioning systems, J. Clean. Prod. 329 (2021) 129754, https://doi.org/10.1016/j.jclepro.2021.129754.
[18] M. Wilks, C. Wang, J. Ling-Chin, X. Wang, H. Bao, Thermochemical energy storage for cabin heating in battery powered electric vehicles, Energy Convers. Manag. 291 (2023) 117325, https://doi.org/10.1016/j.enconman.2023.117325.
[19] G. Zhang, H. Zou, F. Qin, Q. Xue, C. Tian, Investigation on an improved heat pump AC system with the view of return air utilization and anti-fogging for electric vehicles, Appl. Therm. Eng. 115 (2017) 726–735, https://doi.org/10.1016/j.applthermaleng.2016.12.143.
[20] Y.N. Zhang, R.Z. Wang, T.X. Li, Experimental investigation on an open sorption thermal storage system for space heating, Energy 141 (2017) 2421–2433, https://doi.org/10.1016/j.energy.2017.12.003.
[21] Z. Zhang, W. Li, C. Zhang, J. Chen, Climate control loads prediction of electric vehicles, Appl. Therm. Eng. 110 (2017) 1183–1188, https://doi.org/10.1016/j.applthermaleng.2016.08.186.
[22] Ziqi Zhang, D. Wang, C. Zhang, J. Chen, Electric vehicle range extension strategies based on improved AC system in cold climate – a review, Int. J. Refrig. 88 (2018) 141–150, https://doi.org/10.1016/j.ijrefrig.2017.12.018.
[23] Zhenying Zhang, J. Wang, X. Feng, L. Chang, Y. Chen, X. Wang, The solutions to electric vehicle air conditioning systems: a review, Renew. Sustain. Energy Rev. 91 (2018) 443–463, https://doi.org/10.1016/j.rser.2018.04.005.
[24] L. Zhang, K. Hashimoto, H. Hasegawa, M. Saikawa, Performance analysis of a heat pump system with integrated desiccant for electric vehicles, Int. J. Refrig. 86 (2018) 154–162, https://doi.org/10.1016/j.ijrefrig.2017.10.036.
[25] Y. Zhang, R. Wang, Sorption thermal energy storage: concept, process, applications and perspectives, Energy Storage Mater. 27 (2020) 352–369, https://doi.org/10.1016/j.ensm.2020.02.024.
[26] G. Zhou, H. Li, E. Liu, B. Li, Y. Yan, T. Chen, X. Chen, Experimental study on combined defrosting performance of heat pump air conditioning system for pure electric vehicle in low temperature, Appl. Therm. Eng. 116 (2017) 677–684, https://doi.org/10.1016/j.applthermaleng.2017.01.088.